Journal Pre-proof

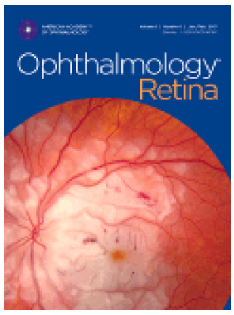

Enhanced S-cone syndrome: spectrum of clinical, imaging, electrophysiological and genetic findings in a retrospective case series of 56 patients

Emanuel R. de Carvalho, Anthony G. Robson, Gavin Arno, Camiel Boon, Andrew A. Webster, Michel Michaelides

PII: S2468-6530(20)30286-4

DOI: https://doi.org/10.1016/j.oret.2020.07.008

Reference: ORET 847

To appear in: *Ophthalmology Retina*

Received Date: 9 May 2020

Revised Date: 6 July 2020

Accepted Date: 9 July 2020

Please cite this article as: de Carvalho E.R., Robson A.G., Arno G., Boon C., Webster A.A. & Michaelides M., Enhanced S-cone syndrome: spectrum of clinical, imaging, electrophysiological and genetic findings in a retrospective case series of 56 patients, *Ophthalmology Retina* (2020), doi: https://doi.org/10.1016/j.oret.2020.07.008.

Enhanced S-cone syndrome: spectrum of clinical, imaging, electrophysiological and genetic findings in a retrospective case series of 56 patients

Enhanced S-cone syndrome: spectrum of clinical, imaging, electrophysiological and genetic findings in a retrospective case series of 56 patients

Emanuel R. de Carvalho[a,b], Anthony G. Robson[a,b], Gavin Arno[a,c], Camiel Boon[b,d], Andrew A. Webster[a,c], Michel Michaelides[a,c]

[a] Moorfields Eye Hospital, City Road, London, United Kingdom
[b] Department of Ophthalmology, Amsterdam University Medical Centers, Amsterdam, the Netherlands
[c] UCL Institute of Ophthalmology, University College London, London, United Kingdom
[d] Department of Ophthalmology, Leiden University Medical Center, Leiden, the Netherlands

Conflict of Interest: No conflicting relationship exists for any author.

Corresponding Author:
Professor Michel Michaelides, MD, FRCOphth
UCL Institute of Ophthalmology, London EC1V 9EL, United Kingdom
Email: michel.michaelides@ucl.ac.uk

Financial Support: Supported by grants from the National Institute for Health Research Biomedical Research Centre at Moorfields Eye Hospital NHS Foundation Trust and UCL Institute of Ophthalmology, Fight for Sight, Moorfields Eye Charity, Retina UK, and the Foundation Fighting Blindness (USA).

Running Head: Clinical Spectrum of Enhanced S-Cone Syndrome

This article contains additional online-only material. The following should appear online-only: Supplemental Figures 1 and 2 and Supplemental Tables 1 and 2.

Abstracf

Purpose: To describe the detailed phenotype, long-term clinical course, clinical variability, and genotype of patients with Enhanced S-Cone Syndrome (ESCS).

Design: Retrospective case series.

Participants: Fifty-six patients with ESCS.

Methods: Clinical history, examination, imaging and electrophysiological findings of 56 patients (age range 1 – 75 years) diagnosed with ESCS were reviewed. Diagnosis was established by molecular confirmation of disease-causing variants in the *NR2E3* gene (n = 38) or by diagnostic full-field electroretinography (ERG) findings (n = 18).

Main outcome measures: Age at onset of visual symptoms, best-corrected visual acuity (BCVA), quantitative age-related electrophysiological decline and imaging findings.

Results: The mean age at onset of visual symptoms was 4.0 years, and median age at presentation was 20.5 years, with the mean follow-up interval being 6.1 years. Six patients were assessed once. Disease-causing variants in *NR2E3* were identified in 38 patients. The mean logMAR BCVA of the better-seeing eye was 0.32 at baseline and 0.39 at follow-up. BCVA remained stable in the majority of eyes (76%, 76/100), with a mean BCVA change of 0.07 logMAR during follow-up. Nyctalopia was the commonest initial symptom, reported in 92.9% (52/56) of patients. Clinical findings were highly variable, and included foveomacular schisis (41.1%, 26/56), yellow/white dots (57.1%, 32/56), nummular pigmentation (85.7%, 48/56), torpedo-like lesions (10.7%, 6/56) and circumferential subretinal fibrosis (7.1%, 4/56). Macular and peripheral patterns of autofluorescence were classified as (i) minimal change, (ii) hypoautofluorescent (mild diffuse; moderate speckled; moderate diffuse; advanced), or (iii) hyperautofluorescent flecks. One patient had undetectable ERGs; quantification of the main ERG components in all other patients revealed amplitude and peak time variability, but with pathognomonic ERG features. The main ERG components showed

evidence of age-related worsening over 6.7 decades, at a rate indistinguishable from that seen in unaffected control subjects. Eighteen sequence variants in *NR2E3* were identified, including four novel missense changes.

Conclusions ESCS has a highly variable phenotype with relative clinical and imaging stability over time. The ERGs have pathognomonic features in most, but quantitative assessment reveals variability and a normal mean rate of age-related decline, consistent with largely non-progressive peripheral retinal dysfunction.

Introduction

Enhanced S-Cone Syndrome (ESCS) (OMIM 268100) is an autosomal-recessive retinal dystrophy caused by disease-causing variants in nuclear receptor subfamily 2, group E, member 3 (*NR2E3*), a member of the nuclear hormone receptor superfamily of ligand-modulated transcription factors; also known as photoreceptor-specific nuclear receptor (PNR; OMIM 604485).[1-4] Goldmann-Favre Syndrome has also been shown to be caused by biallelic variants in *NR2E3*, rendering distinction between the two entities redundant.[5-9] Similarly, recessive variants in *NR2E3* have been described in cases of clumped pigmentary retinal degeneration.[6] A single missense *NR2E3* variant (p.G56R) has also been linked to autosomal dominant retinitis pigmentosa (OMIM 611131).[10, 11]

NR2E3 was first identified by its homology to *NR2E1*, which acts on cell-fate determination in *Drosophila* and encodes an orphan receptor of the steroid/thyroid hormone receptor superfamily of ligand-activated transcription factors.[12, 13] In the eye, *NR2E3* regulates the fate of retinal progenitor cells during retinogenesis.[14-17] The different cell subtypes in the vertebrate retina derive from a common population of multipotent progenitors.[18, 19] Cone primordial cells arise earlier than rod cells.[16, 20] Cellular interactions between cones dictate the ensuing spatial rearrangement, opsin expression, and ratio of photoreceptor subtypes in the mature retina. Disease-causing variants in *NR2E3*, expressed in late retinal progenitors and differentiating photoreceptors in the outer nuclear layer of the retina, disrupt the determination of photoreceptor cell-fate, affecting the normal ratio and topographical distribution of the different photoreceptor subtypes in the mature retina.[21, 22] S-cones are expressed earlier than M (medium wavelength)- and L (long wavelength)- cone photoreceptors and are therefore regarded as the default primordial cone cells.[22] As a result, in the absence of *NR2E3*, rods develop into non-functional hybrid photoreceptors and L- and M-cone expression is suppressed with a concomitant over-expression of ancestral S-cones.[22 15, 16, 20, 23-25]

The unique photoreceptor arrangement in patients harboring *NR2E3* variants is responsible for the increased sensitivity to blue light[26] and is often reflected by pathognomonic full-field electroretinography (ERG) responses. The dark-adapted (DA) rod-specific dim flash (DA0.01) ERG is typically undetectable; although detectable responses have been reported in mild ESCS, which has been suggested to stem from functional dimerization of *NR2E3* mediated by ligand-binding domain variants.[27-29] Responses in the retina are dominated by short-wavelength-sensitive mechanisms, leading to a similar simplified and severely delayed waveform under DA and light-adapted (LA) conditions, with a severely abnormal LA30Hz flicker ERG.[21, 30-33, 90] Short-wavelength-specific stimulation may elicit a high amplitude response when compared to those of normal subjects, consistent with the increased number of S-cone photoreceptors.[23]

Previously reported symptoms of patients with ESCS include nyctalopia, variable visual acuity loss and constricted field of vision.[33-35] The clinical signs encompass a combination of yellow/white dots, nummular pigmentation at the level of the retinal pigment epithelium (RPE), especially along the temporal vascular arcades, and variable degrees of foveomacular schisis.[31, 33, 35-40] Other signs include torpedo-like retinal lesions, cystoid macular edema and circumferential subretinal fibrosis, the latter thought to occur secondary to choroidal neovascularization.[41, 42] Although clinical and electroretinographic characteristics are well-recognised, published analyses are often qualitative and there is a lack of data relating to the natural history of the disorder.

The purpose of the present study was to retrospectively review clinical and electrophysiological data of a large cohort of patients diagnosed with ESCS to better define variability of the phenotype, long-term visual outcome, severity and stability of retinal dysfunction, and the nature of *NR2E3* disease-causing variants.

Patients and methods

A cohort of 56 patients with a clinical diagnosis of ESCS were ascertained at Moorfields Eye Hospital (n = 45) and at the Expertise Center for Hereditary Retinal Diseases of Amsterdam University Medical Centers/Leiden University Medical Center (n = 11), with a mean follow-up time of 6.1 years (range 0 – 34 years). All patients were first diagnosed between 1984 and 2018, with the latest examination performed in 2019. A baseline ERG was performed in 31 patients and repeated in 3 patients. The cohort included 3 cases of pseudo-dominance with consanguineous parents, and 5 sibships (4 sibling pairs, 1 sibling pair with an affected parent, and 2 pairs of 1 affected parent and 1 affected child). Molecular confirmation of the diagnosis was established in 43 patients, and 24 of these underwent baseline ERGs. The diagnosis was established on pathognomonic ERG responses and phenotypical retinal changes in the remaining 13 patients. The protocol of the study adhered to the tenets of the Declaration of Helsinki and was approved by the Ethics Committee of all involved institutions. Thirteen cases were described previously but without detailed ERG quantification and longitudinal data.[33, 43, 44]

Clinical Assessment

Fifty-six patients were ascertained. Six patients were assessed on a single occasion, and all others on at least 2 occasions. In the latter group, the initial and last visits were taken as baseline and follow-up examinations, respectively. Follow-up time was determined by the interval between age at baseline and age at the latest follow-up examination.

Color contrast sensitivity was assessed in 12 patients along tritan, protan and deutan axes using the “ChromaTest”, involving the use of colored optotypes presented on a randomized luminance noise background.[45, 46] In all patients, a medical history was obtained and a comprehensive ophthalmologic examination performed which included best-corrected Snellen

visual acuity converted to equivalent logarithm of minimal angle of resolution (logMAR) for the purpose of data analysis.[47] Retinal fundus photographs were obtained by conventional 35° fundus color photographs (Topcon Europe Medical BV, Capelle aan den IJssel, the Netherlands) or wide-field confocal scanning laser imaging (Optos PLC, Dunfermline, UK). Spectral-domain optical coherence tomography (SD-OCT, Heidelberg Engineering, Heidelberg, Germany) macular scans were performed in all patients.

The patterns of macular and peripheral fundus autofluorescence (FAF) were assessed in 49 pairs of eyes. Macular FAF images were obtained using a confocal scanning laser ophthalmoscope with blue light excitatory beam (Spectralis, Heidelberg Engineering). When available, peripheral FAF was analyzed with wide-field Optos imaging with green light excitatory beam. Specific macular and peripheral FAF patterns were classified as: (i) no change; (ii) hypoautofluorescence - minimal change pattern, mild diffuse, moderate speckled, moderate diffuse (mid-peripheral half-ring or ring ≤ 5000µm widest diameter), moderate diffuse > 5000µm hypoautofluorescence, nummular (patchy); and (iii) hyperautofluorescent flecks.

Electrophysiology

A total of 32 patients underwent electrophysiological assessment at Moorfields Eye Hospital (age range 6 – 73 years at the time of testing). The electrophysiological assessment included full-field ERG and pattern electroretinography (PERG), incorporating the minimum standards of the International Society for Clinical Electrophysiology of Vision (ISCEV)[48, 49] and recorded using gold foil corneal electrodes. Additionally, 28 patients underwent short-wavelength flash ERG (S-cone ERG),[50] obtained using a blue stimulus (445 nm, 80 cd/m^2; stimulus duration 5 ms) on a constant orange background (620 nm, 560 cd/m^2).[33] S-cone ERG peak times were measured to the second or single positive peak; amplitudes were measured

from baseline to the single or second positive peak[50] or, if an early negative trough was present, as a trough to peak amplitude to better characterize the magnitude of responses.

The patient data were compared with the control (normative) electrophysiological data obtained from 160 healthy subjects (age range 10 – 79 years) which included validated recordings for DA0.01 (n = 117), DA 10.0 (n = 141), LA 3.0 30 Hz (n = 131), and the LA 3.0 (single flash cone) ERG (n = 109).

The amplitude and peak time ratios between the LA 3.0 ERG a-wave and LA 30 Hz were calculated for each patient and these and other main ERG components compared with age and the control data.

A total of 3 patients seen at the Amsterdam University Medical Centers underwent baseline electrophysiological assessment. Electrophysiological data concerning these patients were excluded from analysis, given that flash ERGs were performed according to older or abbreviated protocols using silver thread electrodes, precluding comprehensive ERG phenotyping and direct comparison with ISCEV-standard recordings.

Genetic screening

Patients were screened for disease-causing variants by direct sequencing of all 8 exons and intron-exon boundaries of *NR2E3*. Subsequently, available relatives also underwent sequencing. Genomic DNA was isolated from peripheral blood lymphocytes using a kit (Gentra Puregene blood extraction kit; Qiagen). DNA was amplified using specifically designed primers by polymerase chain reaction, and the polymerase chain reaction fragments were sequenced using standard protocols (details are available from the author on request). The likely pathogenicity of novel missense variants was assessed using the predictive algorithms of InterVar [according to the guidelines by the American College of Medical Genetics and Genomics (ACMG) and the Association for Molecular Pathology (AMP) for

interpretation of causality of sequence variants, http://wintervar.wglab.org], PROVEAN (Protein Variation Effect Analyzer (http://provean.jcvi.org/index.php)[52-54] and PolyPhen-2 (http://genetics.bwh.harvard.edu/pph2).[55] Information regarding the domain structure of NR2E3 was retrieved using UniProtKB - Q9Y5X4 (NR2E3_HUMAN). To predict the consequences of the ligand-binding domain missense mutations in the 3-dimensional space, we analyzed the crystal structure of apo NR2E3 ligand-binding domain with pdb code 4LOG, retrieved from the SWISS-MODEL server.[56-59]

Statistical Analysis

The mean, standard error of mean, median, standard deviation and range were used as appropriate. Best-corrected visual acuities (BCVA) were ascertained and converted to logarithm of the minimum angle of resolution (logMAR) scale for statistical analysis.[47] Mean BCVA change over follow-up was calculated per each eye, right and left, using the related samples Wilcoxon signed rank test with $P < 0.05$ deemed clinically significant. Variability between BCVA in the right and left eye recordings at baseline and follow-up was assessed using the paired samples Wilcoxon signed rank test, with $P < 0.05$ deemed clinically significant. Age was correlated with BCVA at baseline and follow-up applying a Spearman correlation model with $P < 0.05$ deemed clinically significant. The relationship between visual acuity and electrophysiological responses was assessed by multiple linear regression analysis and $P < 0.05$ was considered statistically significant. Pearson correlation coefficients were calculated to compare the PERG P50 measure of macular function with central visual acuity and age. Photopic ERG a-wave / 30Hz flicker ratios were compared with unpaired Mann Whitney t-test. Statistical analyses were performed using IBM SPSS ver. 25.0 (IBM Corp., Armonk, NY, USA) and GraphPad Prism 8 (GraphPad Software, San Diego, CA, USA).

Results

Clinical Findings

Fifty-six patients including 33 female (59%) and 23 male (41%) were included. Thirty patients had European ethnic origin (54%), 20 had Middle Eastern ethnic origin (36%), 4 had South Asian ethnic origin (7%) and 2 had Black ethnic origin (3%). Nyctalopia was reported as the first symptom in 52 patients (93%), with or without reduced central visual acuity. The remaining 4 patients described reduced central acuity without nyctalopia as their initial symptom. At presentation, a manifest squint was observed in 9 patients and nystagmus was recorded in 3 patients. Refractive assessment was conducted in 21 patients; hyperopia in 12 (57.1%), myopia in 6 (28.5%) and plano in 3 (14.2%). Color contrast sensitivity was tested in 9 patients; 6 patients had relative sparing of the tritan axis and moderately elevated protan and deutan thresholds, 1 patient had non-specific dyschromatopsia, and 2 had normal results.

The median age at onset of visual symptoms was 4.0 years (range, 0 – 27 years). The median age of presentation to the eye clinic (baseline) and follow-up were 20.5 years (range, 1 – 75 years) and 33.0 years (range, 2 – 81 years), respectively. The mean follow-up interval was 6.1 years (range, 0 – 34 years). Six patients were assessed once. Twenty-eight patients (50%) presented before 21 years of age. Thirteen patients presented after 50 years of age (23%).

The mean logMAR BCVA of the better-seeing eye at baseline and at follow-up were 0.32 [standard error of mean (SEM) 0.045; range, 0.0 – 1.77] and 0.39 (SEM 0.054; range, 0.0 – 1.60), respectively (Table 1). No clinically significant difference was found between BCVA in the right and left eyes (P = 0.14 for baseline BCVA, P = 0.22 for follow-up BCVA). Overall, mean logMAR BCVA change was 0.01 logMAR (SEM 0.05), although this included cases with short follow-up time (< 6 years). In the group with extended follow-up time (≥ 6 years, n = 21) mean logMAR BCVA change was 0.12 (SEM 0.09, Figure 1). A score of

BCVA severity was attributed for each eye and progression over time was assessed for each eye separately. Severity was graded as very mild (logMAR BCVA ≤ 0.1, n = 7, 12.5%), mild (≤ 0.3, n = 21, 37.5%), moderate (≤ 0.6, n = 12, 21.4%), severe (≤ 1, n = 11, 19.6%) and very severe (> 1.0, n= 5, 9%). No progression was observed in 79 of 100 eyes. Ten eyes progressed from very mild and mild severity scores to moderate severity (10%). Five eyes progressed from mild and moderate severity scores to severe (5%), and six eyes progressed from severe to very severe (6%). Poor visual acuity (logMar BCVA > 0.6) was observed in 16 patients at baseline (28.5%, median age 29.0 years, range, 0.5 – 51 years) and in 18 patients at last follow-up (36%). In two patients, BCVA loss in one eye could be directly attributed to other significant ophthalmic events, namely retinal detachment and dense amblyopia. In five other patients, BCVA loss could be partly ascribed to concurrent ophthalmic pathology. In one patient with undetectable cone and rod ERG responses, optic disc pallor was observed at initial presentation. The patient was assessed by neuro-ophthalmology and no underlying neuro-ophthalmic aetiology was found for the optic neuropathy. In 6 patients with documented BCVA worsening over time, no other unrelated significant ophthalmic events were reported. The majority of patients (13/18) with severe visual outcomes had moderate to advanced foveomacular schisis with accompanying or ensuing macular atrophy in 8 patients. Three patients presented with advanced macular atrophy at initial visit. Cystoid macular edema was confirmed on fluorescein angiography in one patient, and diagnosed based on structural OCT appearance in three other patients with severe visual outcomes. Treatment with oral carbonic anhydrase inhibitors was attempted in 4 patients, with a positive anatomical response attained in two patients, albeit with no visual improvement noted post-treatment. One patient was diagnosed with congenital nystagmus at birth, with delayed visual development that might have contributed to poor visual outcome. There was no significant

correlation between PERG responses and clinical severity. Clinical findings are summarized in Tables 1, 2 and 3.

Clinical and Fundus Autofluorescence Features

Clinical notes, imaging data and color fundus photographs were reviewed in all patients.

In most cases, yellow-white dots and/or nummular pigmentation were observed, located within the vascular arcades in 16 patients (28.6%), and in the mid-peripheral retina, outside the vascular arcades in 49 patients (87.5%, Figure 2A-E). Nummular pigmentation, characterized by deep round-shaped pigmentation at the level of the RPE, was usually located in the mid-peripheral retina, along the vascular arcades and often associated with RPE atrophy and end-stage hypoautofluorescence (Figure 4J). This was the most common clinical finding, present in 48 patients (85.7%), followed by yellow-white dots which were seen in 32 patients (57.1%). The combined presence of nummular pigmentation with yellow dots was observed in 26 patients (46.4%). Two patients developed clumped and nummular pigmentary changes in an area of the mid-peripheral retina with yellow-white dots (Figure 2K, L).

Other clinical findings included vitreous opacities (21.4%), peripheral torpedo-like lesions (10.7%, Figure 2F), circumferential subretinal fibrosis (7.1%, Figure 2G), optic disc pallor (5.4%), and recurring vitreous hemorrhages secondary to pre-retinal neovascularization in one patient (1.8%, Figure 2I). Color fundus photographs and optical coherence tomography scans of a representative group of patients depict the above-mentioned clinical features in Figures 2 and 3.

Foveomacular schisis was identified in 23 of 56 patients (41%, Figure 3B and 3C). Two patients developed giant foveomacular schisis (Figure 3D), which evolved into advanced macular atrophy in one eye (Figure 3F and 4E). In all other patients, OCT appearances were relatively stable. The schitic cavities were located at the level of the inner nuclear layer,

characterized by a round shape, and in the outer nuclear layer (ONL) where they appeared elongated in a stellate-like configuration (Figure 3C). A total of 16 patients (28.6%,) were diagnosed with presumed cystoid macular edema (CME), based on structural appearance on SD-OCT. Four cases were treated with oral carbonic anhydrase inhibitors. Resolution of CME was attained in two patients, albeit with no visual gain, including in the single patient where, prior to treatment, leakage had been demonstrated on fluorescein angiography.

The majority of patients (55%) presented with minimal autofluorescent changes at the level of the macula (minimal change pattern), combined with the presence of hyperautofluorescent flecks in some cases. End-stage macular atrophy with secondary severe macular hypoautofluorescence was observed in one patient and this was preceded by giant foveomacular schisis. The hyperautofluorescent flecks correlated with the presence of yellow/white dots (Figure 4K and 4L). In the peripheral retina, moderate decrease in autofluorescence was observed in the majority of patients (31.7%), usually combined with patchy severe hypoautofluorescence, the latter corresponding to the presence of nummular pigmentary deposition. A strong half-ring of pronounced hyperautofluorescence along the temporal macular rim was observed in all cases presenting with peripheral half-ring hypoautofluorescence. In 5 patients, the peripheral FAF pattern progressed from moderate decrease in autofluorescence to patchy decrease in autofluorescence, with documented progression of pigmentary changes. Clinical FAF patterns are shown in Figure 4 and summarized in Supplemental Table 1 (available at https://www.ophthalmologyretina.org), where the mean BCVA is presented in relation to the pattern of macular FAF.

Electrophysiological Findings

The PERG P50 component (Supplemental Figure 1, available at https://www.ophthalmologyretina.org) was undetectable (n = 11), delayed and reduced (n =

11), delayed and of normal amplitude (n = 3; see Figure 5 for an example) or normal (n = 3). The threshold values for the PERG P50 minimum amplitude/maximum peak time are presented in Supplemental Table 2 (available at https://www.ophthalmologyretina.org). There was no correlation between the PERG P50 amplitude and visual acuity in right (r= -0.20, P = 0.277; n = 31) or left eyes (r = -0.18, P = 0.326; n = 31). There was significant negative correlation between age and PERG P50 amplitude for right (r = 0.65, $P < 0.05$; n = 36) and left eyes (r = 0.6; $P < 0.05$) and positive correlation between age and P50 peak time for right (r = 0.6; $P < 0.05$; n = 23) and left eyes (r = 0.55; $P < 0.05$).

The full-field ERG waveforms were undetectable in one patient with a genetically confirmed diagnosis. All other individuals that underwent ISCEV-standard testing (n = 31) had pathognomonic ERG abnormalities, as described below (typical recordings are shown in Figure 5). The DA3.0, DA10.0 and LA3.0 ERGs had a similar simplified and delayed waveform shape. The ranges of full-field ERG component amplitudes and peak times are compared with those in a control group in Figures 6 and 7. The rod-specific (DA0.01) ERG was undetectable in all but one patient (age 14 years) with a detectable but subnormal response (reduction 58% compared with the mean for the control group). The DA10.0 ERG a- and b-wave mean amplitudes were reduced by 52% and 63% respectively and mean a- and b-wave peak times were 16 ms and 14 ms longer respectively compared with those for the control group (Figure 6).

The LA 30Hz ERG and LA3.0 ERG a- and b-wave amplitudes were on average 93%, 28% and 69% lower respectively and mean peak times 14 ms, 8 ms and 20 ms greater respectively compared with mean values for the control group (Figure 7). The LA30Hz flicker ERG was smaller than the LA3.0 ERG a-wave in the majority (n = 48 eyes of 27 subjects) and of equal amplitude to the LA3.0 ERG a-wave in others (n = 9 eyes of 7 subjects) including the 4 eyes with the smallest detectable responses. The mean amplitude ratio between the LA3.0 ERG a-

wave and LA30Hz ERG was 1.86 (n = 30; 44.53% coefficient of variation, SD = 0.9, Figure 8) in the ESCS cohort and 0.37 (n = 111, 24.38% coefficient of variation, SD = 0.09) in the healthy controls. The peak time ratio between the LA3.0 ERG a-wave and LA30Hz ERG was 0.55 (n = 30, 14.02 % coefficient of variation, SD = 0.08, Figure 8) in the ESCS cohort (P = 0.0001) and 1.85 (n = 42, 5.0 % coefficient of variation, SD = 0.09) in the healthy controls.

The mean S-cone ERG amplitude in the ESCS patients was greater (mean 81 µV, median 54 µV, n = 28, mean age 27 years) than in the control group (mean 43.35 µV, median 43 µV, n = 51, mean age 29 years, Figure 9A) and peak times were severely delayed (mean peak time difference (ESCS - control) = 28.3 ms, Figure 9B). S-cone ERGs in ESCS were largest in some of the children and young adults but there was no significant correlation between amplitude or peak time and age (r^2 = 0.06 and r^2 = 0.001 respectively, $P > 0.05$, Figures 9A,9B). In ESCS there was significant correlation between the S-cone ERG and LA3 ERG b-wave amplitudes (r^2 = 0.56, $P < 0.001$) and peak times (r^2 = 0.34, $P < 0.05$, Figures 9C, 9D).

Plots of the major ISCEV-standard ERG component amplitudes and peak times against age are shown in Figures 6 and 7 . There was evidence of age related ERG reduction in the DA and LA ERGs at a rate that was indistinguishable from that seen in healthy subjects, over 6.7 decades (LA3.0 ERG a-wave, r^2 =0.22, P = 0.006; LA3.0 ERG b-wave, r^2 = 0.22, P = 0.007; DA10 a-wave, r^2 = 0.17, P = 0.02 and DA10 b-wave, r^2 = 0.16, P = 0.03). The peak times of the major ERG components in ESCS showed high stability with increasing age, as in the control group.

The patient with compound heterozygous changes in *NR2E3* (c.119-2A>C and the novel p.L303P) had a particularly severe clinical phenotype with early onset of visual symptoms, severely reduced visual acuity (1.0 logMAR), sensory nystagmus and giant foveomacular schisis which evolved into end-stage macular atrophy (Supplemental Figure 2, available at https://www.ophthalmologyretina.org). His ERGs, performed at the age of 53, differed from

all other patients, characterized by undetectable DA and LA ERGs and an undetectable PERG.

Five individuals underwent follow-up ERG testing after intervals of 4, 6, 9, 10 and 17 years. The mean annual rate of ERG reduction (averaged between eyes) for DA10 ERG a- and b-wave amplitudes was 1.6% (range 0-6.0 %) and 3.9% (range 0-6.2 %) respectively; for LA3 ERG a- and b-wave amplitudes the mean rate of reduction was 3.4% (range 2.0-4.7 %) and 1.3% (range 0-2.0 %) respectively.

Molecular Genetics

Forty-one out of 56 patients underwent screening of the nine coding exons of *NR2E3*. Disease-causing variants were identified in 41 subjects. Twenty-four subjects were homozygous and 17 had compound heterozygous variants. Eighteen sequence variants were identified, including four novel missense variants (p.F71L, p.R247W, p.L303P, p.R309Q) (Table 4). The other reported variants encompassed two splice acceptor variants in intron 1 (c.119-2A>C[22] and c.119-3C>G[33]), ten missense mutations (p.R76Q[22], p.C83Y[60], p.A102D[44], p.R104W[22], p.G216S, p.R104Q[27], p.R311Q[16], p.A256E[5], p.V342A[44], p.L371W[61]), one frameshift mutation (p.P399Qfs*3[44]) and a 9-bp deletion leading to deletion of 3 amino acid residues (p.C67_G69del[16]).

The p.G216S substitution (c.646G>A; exon 5) was found as a homozygous change in one patient. This variant, predicted to be benign, is rare in gnomAD, but the amino acid change is not predicted to be damaging by any of the in silico tools utilised. This, however, may be irrelevant to causality. The variant introduces an exonic splice acceptor site: TGCGGCC > tgcagCC (human splice finder [HSF] score: 91.23, nnsplice score 0.97) into exon 5 which is likely to lead to an out of frame deletion of the 5' 77bp of exon 5 and thus may represent a loss of function allele. Without mRNA analysis of relevant patient tissue, it is not possible to

determine if this predicted splice altering effect is indeed occurring in vivo or if any normally spliced transcript would escape and produce functional protein but we are of the opinion that the case for causality is sufficient for this rare variant.

Four novel disease-causing variants were identified. These are likely to be pathogenic given that all are located within highly conserved domains critical to protein function, and all are rare or absent from control datasets. The p.F71L substitution (c.211T>C; exon 2) was found as a heterozygous change in one patient. The p.R247W substitution (c.739C>T; exon 5) was found as a heterozygous change in one patient. The p.L303P substitution (c.908T>C; exon 5) was found as a heterozygous change in one patient. The p.R309Q substitution (c.926G>A; exon 6) was found in a homozygous state in two affected siblings. The Phe71, Arg247, Leu309 and Arg309 are highly conserved across NR2E3 orthologues. NR2E3 has the evolutionarily conserved modular structure of nuclear receptors, namely a highly conserved DNA-binding domain that specifically binds to consensus binding sites located in promoters of target genes, and a ligand-binding domain.[12, 13, 62] Three of the afore-mentioned novel mutations, p.R247W, p.L303P and p.R309Q, are located in the evolutionary-conserved ligand binding domain of *NR2E3*, in helices 4 and 7, causing a rearrangement of the bulky side chains and loss of some hydrogen bonds, suggesting a reduction of protein stability (Figure 10). The p.F71L is located in the evolutionary-conserved DNA binding domain of *NR2E3*.[59, 63] Definite confirmation of the pathogenicity of the four novel variants remains dependent on functional studies that would assess the effects of these sequence variants with regards to *NR2E3* stability, targeting, and ability to interact reversibly and effectively with DNA or ligands.

Discussion

This study describes the largest cohort of patients diagnosed with ESCS. We characterize the clinical variability, and describe molecular characteristics, including four novel variants in *NR2E3*. Detailed quantification of the electrophysiological findings characterizes the phenotypic variability of pathognomonic ERG features and assesses the relative stability of macular and retinal dysfunction over 6 decades, pertinent to possible future interventional studies.

ESCS is characterized by early onset of visual symptoms. In this cohort, all but two patients experienced symptoms in the first two decades of life, with the majority presenting in childhood. Nyctalopia, with or without reduced central visual acuity, was the most frequently described initial complaint. Hyperopia with a variable degree of astigmatism was the most common refractive error, in accordance with other reports.[5, 33, 64]

Sparing along the tritan axis was demonstrated in six patients that underwent color contrast sensitivity testing, suggesting preservation of short-wavelength discrimination. This is also consistent with the high amplitude S-cone ERGs seen in many individuals and with high correlation between S-cone ERGs and LA3 ERGs, likely having identical S-cone-opsin-mediated origins.

Visual function was highly variable amongst patients, ranging from normal to severely reduced (2.0 logMAR). It is noteworthy that in most patients, BCVA remained relatively stable throughout follow-up with no clinical progression observed in 79 of 100 eyes. The slight deterioration in BCVA with increasing age may be ascribed to the expected age-related decline in the general population. In two cases, poor visual outcome was related to non-dystrophic significant ophthalmic events (retinal detachment and dense amblyopia). Poorer visual outcomes were associated with the presence of moderate to advanced (giant) foveomacular schisis, but no other association was found, neither with age at onset of visual symptoms, nor with genotype or electrophysiological responses. There was also a high degree

of interocular symmetry, which could enable the use of the contralateral eye as a valid untreated control in future therapeutic trials in which one eye received treatment.

In the family demonstrating a pseudo-dominance pattern, clinical severity was highly variable. While the father was found to have severely reduced BCVA in both eyes when first assessed at the age of 17, his children had mildly reduced BCVA when tested at an equivalent age. Interestingly, clinical presentation was not only variable within the same family, but also observed in patients from different families harboring the same variant, suggesting that modifier genes (and environmental factors) may modulate disease outcome.[26, 65]

One patient developed bilateral non-diabetic pre-retinal neovascularization and a midperipheral vasoproliferative lesion in one eye which led to recurrent vitreous hemorrhages (Figure 2I). This is an unusual finding and it remains unanswered whether this is related to the underlying retinal dystrophy. Choroidal neovascularization (CNV), on the other hand, has been previously described in patients with ESCS. Asymptomatic development of CNV has also been linked to the presence of torpedo-like lesions and circumferential subretinal fibrosis, both infrequent findings in ESCS.[40, 66-68]

Clinical appearance was highly variable, however, three consistent clinical signs were observed in a large proportion of patients, yellow/white dots, nummular pigmentation at level of the RPE, and foveomacular schisis. In the appropriate clinical context, the presence of these combined features should raise the strong possibility of ESCS.

The yellow/white dots are often characterized by an increase in autofluorescence signal and present in both the macula and midperiphery at the level of the RPE. Histological analysis of autofluorescent white dots seen across the retina of the *rd7* mouse, which harbors a homozygous deletion in *NR2E3*, showed that the autofluorescence signal arose mostly from macrophages, which were associated with whorls and rosettes of dysplastic photoreceptors in

the outer nuclear layer.[69] Further *in vivo* studies are warranted to ascertain the exact origin of the hyperautofluorescent dots observed in ESCS patients.

Nummular pigmentary deposition alone is not specific to ESCS, and has been described in other retinal dystrophies such as Bardet-Biedl syndrome,[70] *CRB1*-associated early-onset severe retinal dystrophy,[71] retinitis pigmentosa with preserved para-arteriolar RPE (*RP12*, associated with *CRB1*)[72] and thioridazine retinopathy.[73] Whenever present, nummular pigmentary deposition was associated with disorganization of the neurosensory retina, including marked loss of the ellipsoid zone and absence of autofluorescence, in keeping with previous reports.[23, 33, 35] In some patients with mid-peripheral, nummular pigmentation, clumped pigmentary deposition was observed. The presence of yellow/white dots has been proposed as a harbinger of more marked pigmentary changes, developing early in the pathogenesis of the disease, followed by the development of nummular and clumped pigmentary deposition at a later stage.[5] Corroborating this assumption, documented progression of pigmentary changes over time was observed in two patients with extended follow-up. The development of pigmentary changes occured independent of age. In our cohort, clumped or nummular pigmentary deposition, although skewed towards older subjects, was present in 11 young patients (age ≤ 20) and absent in 4 older patients (age > 20), corroborating the high variability of clinical phenotype.

The scarcity of fundus fluorescein angiography in the diagnosis of CME poses an important limitation, as we are unable to confirm this solely based on SD-OCT structural appearance. It is possible that the presumed CME documented in many patients represents a variant of foveomacular schisis that mimics the appearance of cystoid spaces. A positive anatomical response to carbonic anhydrase inhibitors was observed in solely two patients although this did not translate into a significant gain in subjective and objective visual function. Notwithstanding, poorer visual outcomes were associated with macular changes, namely

foveomacular schisis, presumed CME and macular atrophy, rendering prevention and treatment of maculopathy an invaluable target in future treatment strategies.

Pattern ERGs ranged from undetectable (indicating severe macular dysfunction) in a large minority to normal (3 of 28 cases), with a higher incidence of P50 delay (Figure 5) than in many other forms of maculopathy. The PERG P50 did not correlate with BCVA, highlighting the value of objective assessment of macular function, likely to be of relevance in the selection of candidates considered amenable to possible future therapeutic interventions.

All but 3 eyes of 2 molecularly confirmed patients had pathognomonic ERG features consistent with ESCS. The full-field ERG findings in the large majority quantified the magnitude, severity and variability of pathognomonic ERG abnormalities, pertinent to diagnostic accuracy and precise phenotyping. The rod-system specific (DA0.01) ERG was undetectable in all but one individual, consistent with a lack of rod function, and the delayed and simplified stronger flash (DA3.0 and DA10.0) ERGs had qualitative similarities to the LA3.0 ERG. In any healthy (control) subject, the LA30Hz ERG peak to peak amplitude is greater than the LA3.0 ERG a-wave and smaller than the LA3 ERG b-wave.[72,73] The LA30Hz ERG is smaller than the LA3 single-flash cone ERG a-wave in ESCS, as previously reported, and relating to the minimal contribution of the (relatively slow) S-cone system to the 30Hz flicker response,[5960] The current study highlights both the variability and high specificity of this feature; the LA3 a-wave to LA30Hz ERG amplitude ratio was never less than 1.0 and the lowest ratios (1.0) included cases with grossly reduced ERGs associated with a lower signal:noise ratio. Furthermore, relatively increased sensitivity to short-wavelength stimulation was observed, as demonstrated by large, delayed and simplified S-cone ERG responses or S-cone ERGs that were larger than the corresponding LA3 ERGs. The S-cone ERGs are not required for the diagnosis of ESCS, but the high correlation with the LA 3.0 ERGs, is consistent with both having the same S-cone-dominated origin.

All but 3 eyes of 2 molecularly confirmed patients had the above-mentioned pathognomonic ERG features, in accordance with previous reports demonstrating that solely patients found to harbor mutations in *NR2E3* have pathognomonic ERG responses when compared to patients with retinal dystrophies unrelated to *NR2E3*.[5] Thus, in our cohort, the presence of clinical features consistent with ESCS alongside typical ERG responses were deemed diagnostic for ESCS, irrespective of molecular confirmation.

A comparison of multiple ERG component amplitudes with age, suggests a low mean rate of reduction over more than 6 decades, with no evidence of worsening beyond that explained by age. This finding highlights the relative stability of peripheral retinal function in most ESCS patients, and may be an important prognostic consideration for retention of peripheral retinal function. Marked inter-subject variability is evident with some younger adults showing markedly reduced ERG amplitudes, highlighting the importance of detailed phenotyping and need to manage cases individually. Peak times of the main ERG components are delayed but show a similar high level of stability to that in the control group. Longitudinal ERG data were available in three patients, showing relatively stable responses in two patients and mild reduction of both LA and DA function in one.

Four evolutionary conserved domains are identified in the *NR2E3* protein, shared by the nuclear hormone receptor family; the highly variable A/B domain, n terminal DNA binding domain, a flexible hinge region and the ligand-binding and dimerization domain in the C terminus.[74] Most mutations are located within the DNA binding domain and the ligand-binding domain.[2, 3, 5, 16, 26]

Genetic heterogeneity occurs in ESCS. Autosomal recessive variants in the neural retina leucine zipper (*NRL*) gene have been identified in patients presenting with an ESCS-like phenotype.[7, 75-78] This gene had been proposed as a possible candidate following the phenotypical characterization of the *Nrl*$^{-/-}$ mouse which revealed a complete loss of rod

function and super-normal cone function, driven by over-expressed S-cones.[79] Expression of *NR2E3* is almost absent in the *Nrl*$^{-/-}$, implying that *NR2E3* is completely dependent of *NRL* expression.[18] *NRL* encodes a basic-motif leucine zipper DNA binding protein that interacts with the paired-type homeobox transcription factor cone-rod homeobox (*CRX*) and *NR2E3*, driving the differentiation of post-mitotic photoreceptors into the rod lineage.[76-78, 80-82].

The function of genetic modifiers of *NR2E3*, such as the nuclear hormone receptor *Nr1d1* (Rev-erbα), has been explored as a therapeutic option in the *NR2E3*-associated retinal disease, *rd7*, mouse model.[26, 69, 83] Delivery of the *Nr1d1* gene restored the retinal topography of the *NR2E3*$^{rd7/rd7}$ neonates, and re-regulated the expression of key genes involved in phototransduction.[26] Future studies will need to assess whether this approach would be suited for patients with advanced disease.

The present study describes the detailed clinical, imaging, molecular and electrophysiological findings in a cohort of 56 patients with ESCS, which, to the best of our knowledge, is the largest cohort to date. Four novel *NR2E3* variants are identified. The data quantify diagnostic ERG criteria and phenotypic spectrum, with evidence to suggest relative stability of peripheral retinal function over more than 6 decades, and additional evidence suggesting that central visual function remains relatively stable in the majority of patients, which is invaluable for counseling on prognosis. Any future intervention directed at preventing visual decline in ESCS will need to address its impact on the development of macular complications, namely foveomacular schisis and macular atrophy, which are largely responsible for the poor visual outcome observed in a subset of affected patients.

References

1. Kobayashi M, Takezawa S, Hara K, et al. Identification of a photoreceptor cell-specific nuclear receptor. Proc Natl Acad Sci U S A 1999;96(9):4814-9.
2. Schorderet DF, Escher P. NR2E3 Mutations in Enhanced S-Cone Sensitivity Syndrome (ESCS), Goldmann-Favre Syndrome (GFS), Clumped Pigmentary Retinal Degeneration (CPRD), and Retinitis Pigmentosa (RP). Hum Mutat 2009;30(11):1475-85.
3. Coppieters F, Leroy BP, Beysen D, et al. Recurrent mutation in the first zinc finger of the orphan nuclear receptor NR2E3 causes autosomal dominant retinitis pigmentosa. Am J Hum Gen 2007;81(1):147-57.
4. Gerber S, Rozet JM, Takezawa SI, et al. The photoreceptor cell-specific nuclear receptor gene (PNR) accounts for retinitis pigmentosa in the Crypto-Jews from Portugal (Marranos), survivors from the Spanish Inquisition. Hum Genet 2000;107(3):276-84.
5. Sharon D, Sandberg MA, Berson EL, Dryja TP. Shared mutations in NR2E3 in enhanced S-cone syndrome, Goldmann-Favre syndrome, and clumped pigmentary retinal degeneration. Invest Ophthalmol Vis Sci 2002;43:U172-U.
6. Sharon D, Sandberg MA, Caruso RC, et al. Shared mutations in NR2E3 in enhanced S-cone syndrome, Goldmann-Favre syndrome, and many cases of clumped pigmentary retinal degeneration. Arch Ophthalmol 2003;121(9):1316-23.
7. Acar C, Mears A, Yashar B, et al. Mutation screening of patients with Leber congenital amaurosis or the enhanced S-cone syndrome reveals a lack of sequence variations in the NRL gene. Mol Vis 2003;9(3-4):14-7.
8. Jacobson SG, Roman AJ, Roman MI, et al. Relatively Enhanced S-Cone Function in the Goldmann-Favre Syndrome. Am J Ophthalmol1991;111(4):446-53.
9. Jacobson SG, Roman AJ, Roman MI, et al. A Pattern of Retinal Dysfunction That Links the Goldmann-Favre Syndrome with the Enhanced S (Blue) Cone Syndrome. Invest Ophthalmol Vis Sci 1991;32(4):912-.
10. Chavala SH, Sari A, Lewis H, et al. An Arg311Gln NR2E3 mutation in a family with classic Goldmann-Favre syndrome. Br J Ophthalmol 2005;89(8):1065-6.
11. Gire AI, Sullivan LS, Bowne SJ, et al. The Gly56Arg mutation in NR2E3 accounts for 1-2% of autosomal dominant retinitis pigmentosa. Mol Vis2007;13(220-22):1970-5.
12. Kobayashi M, Hara K, Yu RT, Yasuda K. Expression and functional analysis of Nr2e3, a photoreceptor-specific nuclear receptor, suggest common mechanisms in retinal development between avians and mammals. Dev Gen Evol 2008;218(8):439-44.
13. Kobayashi M, Takezawa S, Hara K, et al. Identification of a photoreceptor cell-specific nuclear receptor. PProc Natl Acad Sci U S A 1999;96(9):4814-9.
14. Hood DC, Cideciyan AV, Roman AJ, Jacobson SG. Enhanced S-Cone-Syndrome - Evidence for an Abnormally Large Number of S-Cones. Vis Res1995;35(10):1473-81.
15. Haider N, Naggert JK, Nishina PM. The transcription factor NR2E3 suppresses cone cell proliferation. Invest Ophthalmol Vis Sci 2005;46.
16. Haider NB, Jacobson SG, Cideciyan AV, et al. Mutation of a nuclear receptor gene, NR2E3, causes enhanced S cone syndrome, a disorder of retinal cell fate. Nature Genet 2000;24(2):127-31.
17. Haider NB, Naggert JK, Nishina PM. Elucidating the function of NR2E3 through identification of interacting factors. Invest Ophthalmol Vis Sci 2004;45:U631-U.
18. Cepko CL. The Determination of Rod and Cone Photoreceptor Fate. Annu Rev Vis Sci, Vol 1 2015;1:211-34.
19. Wang S, Cepko CL. Photoreceptor Fate Determination in the Vertebrate Retina. Invest Ophthalmol Vis Sci 2016;57(5).
20. Haider NB, Demarco P, Nystuen AM, et al. The transcription factor Nr2e3 functions in retinal progenitors to suppress cone cell generation. Vis Neurosci 2006;23(6):917-29.

21. Hood DC, Cideciyan AV, Roman AJ, Jacobson SG. Enhanced S cone syndrome: evidence for an abnormally large number of S cones. Vision Res 1995;35(10):1473-81.
22. Haider NB, Jacobson SG, Cideciyan AV, et al. Mutation of a nuclear receptor gene, NR2E3, causes enhanced S cone syndrome, a disorder of retinal cell fate. Nat Genet 2000;24(2):127-31.
23. Milam AH, Rose L, Cideciyan AV, et al. The nuclear receptor NR2E3 plays a role in human retinal photoreceptor differentiation and degeneration. PProc Natl Acad Sci U S A 2002;99(1):473-8.
24. Haider NB, Mollema N, Gaule M, et al. Nr2e3-directed transcriptional regulation of genes involved in photoreceptor development and cell-type specific phototransduction. Exp Eye Res 2009;89(3):365-72.
25. Corbo JC, Cepko CL. A hybrid photoreceptor expressing both rod and cone genes in a mouse model of enhanced S-cone syndrome. PLoS Genet 2005 Aug;1(2):e11.
26. Cruz NM, Yuan Y, Leehy BD, et al. Modifier Genes as Therapeutics: The Nuclear Hormone Receptor Rev Erb Alpha (Nr1d1) Rescues Nr2e3 Associated Retinal Disease. PLoS One 2014;9(1).
27. Hayashi T, Gekka T, Goto-Omoto S, et al. Novel NR2E3 mutations (R104Q, R334G) associated with a mild form of enhanced S-cone syndrome demonstrate compound heterozygosity. Ophthalmology 2005;112(12):2115-22.
28. Lam BL, Goldberg JL, Hartley KL, Stone EM. Atypical mild enhanced S-Cone syndrome with novel compound heterozygosity of the NR2E3 gene. Am J Ophthalmol 2007;144(1):157-9.
29. von Alpen D, Tran HV, Guex N, et al. Differential Dimerization of Variants Linked to Enhanced S-Cone Sensitivity Syndrome (ESCS) Located in the NR2E3 Ligand-Binding Domain. Hum Mut 2015;36(6):599-610.
30. Jacobson SG, Marmor MF, Kemp CM, Knighton RW. SWS (blue) cone hypersensitivity in a newly identified retinal degeneration. Invest Ophthalmol Vis Sci 1990;31(5):827-38.
31. Marmor MF, Jacobson SG, Foerster MH, et al. Diagnostic clinical findings of a new syndrome with night blindness, maculopathy, and enhanced S cone sensitivity. Am J Ophthalmol 1990;110(2):124-34.
32. Greenstein VC, Zaidi Q, Hood DC, et al. The enhanced S cone syndrome: an analysis of receptoral and post-receptoral changes. Vision Res 1996;36(22):3711-22.
33. Audo I, Michaelides M, Robson AG, et al. Phenotypic variation in enhanced S-cone syndrome. Invest Ophthalmol Vis Sci 2008;49(5):2082-93.
34. Corbo JC, Cepko CL. A hybrid photoreceptor expressing both rod and cone genes in a mouse model of enhanced S-cone syndrome. PLoS Genet2005;1(2):140-53.
35. Audo IS, Neveu MM, Robson AG, et al. Characterization of enhanced S-cone Syndrome (ESCS). Invest Ophthalmol Vis Sci 2004;45:U579-U.
36. Jurklies B, Weismann M, Kellner U, et al. Clinical findings in autosomal recessive enhanced S-cone sensitivity syndrome. Ophthalmologe 2001;98(3):285-93.
37. Khan AO, Aldahmesh M, Meyer B. The enhanced S-cone syndrome in children. Br J Ophthalmol 2007;91(3):394-6.
38. Marmor MF. A teenager with nightblindness and cystic maculopathy: enhanced S cone syndrome (Goldmann-Favre syndrome). Doc Ophthalmol 2006;113(3):213-5.
39. Wang NK, Fine HF, Chang S, et al. Cellular origin of fundus autofluorescence in patients and mice with a defective NR2E3 gene. Br J Ophthalmol 2009;93(9):1234-40.
40. Yzer S, Barbazetto I, Allikmets R, et al. Expanded Clinical Spectrum of Enhanced S-Cone Syndrome. JAMA Ophthalmol 2013;131(10):1324-30.
41. Yzer S, Barbazetto I, Allikmets R, et al. Expanded clinical spectrum of enhanced S-cone syndrome. JAMA Ophthalmol 2013;131(10):1324-30.
42. Zerbib J, Blanco Garavito R, Gerber S, et al. Retinochoroidal Anastomosis Associated with Enhanced S-Cone Syndrome. Retin Cases Brief Rep 2017.
43. Vaclavik V, Chakarova C, Bhattacharya SS, et al. Bilateral giant macular schisis in a patient with enhanced S-cone syndrome from a family showing pseudo-dominant inheritance. Br J Ophthalmol 2008;92(2):299-300.
44. Hull S, Arno G, Sergouniotis PI, et al. Clinical and Molecular Characterization of Enhanced S-Cone Syndrome in Children. JAMA Ophthalmol 2014;132(11):1341-9.

45. Arden G, Gunduz K, Perry S. Color-Vision Testing with a Computer-Graphics System - Preliminary-Results. Doc Ophthalmol 1988;69(2):167-74.
46. Arden GB, Wolf JE. Colour vision testing as an aid to diagnosis and management of age related maculopathy. Br J Ophthalmol 2004;88(9):1180-5.
47. Holladay JT. Proper method for calculating average visual acuity. J Refract Surg 1997;13(4):388-91.
48. Bach M, Brigell MG, Hawlina M, et al. ISCEV standard for clinical pattern electroretinography (PERG): 2012 update. Doc Ophthalmol 2013;126(1):1-7.
49. McCulloch DL, Marmor MF, Brigell MG, et al. ISCEV Standard for full-field clinical electroretinography (2015 update). Doc Ophthalmol 2015;130(1):1-12.
50. Perlman I, Kondo M, Chelva E, et al. ISCEV extended protocol for the S-cone ERG. Doc Ophthalmol 2020;140(2):95-101.
51. Li Q, Wang K. InterVar: Clinical Interpretation of Genetic Variants by the 2015 ACMG-AMP Guidelines. Am J Hum Gen2017;100(2):267-80.
52. Choi Y, Chan AP. PROVEAN web server: a tool to predict the functional effect of amino acid substitutions and indels. Bioinformatics 2015;31(16):2745-7.
53. Choi Y, Sims GE, Murphy S, et al. Predicting the functional effect of amino acid substitutions and indels. PLoS One 2012;7(10):e46688.
54. Ng PC, Henikoff S. SIFT: predicting amino acid changes that affect protein function. Nucleic Acids Res 2003;31(13):3812-4.
55. Adzhubei IA, Schmidt S, Peshkin L, et al. A method and server for predicting damaging missense mutations. Nat Methods 2010;7(4):248-9.
56. Bienert S, Waterhouse A, de Beer TAP, et al. The SWISS-MODEL Repository-new features and functionality. Nucleic Acids Res 2017;45(D1):D313-D9.
57. Guex N, Peitsch MC, Schwede T. Automated comparative protein structure modeling with SWISS-MODEL and Swiss-PdbViewer: A historical perspective. Electrophoresis 2009;30:S162-S73.
58. Waterhouse A, Bertoni M, Bienert S, et al. SWISS-MODEL: homology modelling of protein structures and complexes. Nucleic Acids Res 2018;46(W1):W296-W303.
59. Tan MHE, Zhou XE, Soon FF, et al. The Crystal Structure of the Orphan Nuclear Receptor NR2E3/PNR Ligand Binding Domain Reveals a Dimeric Auto-Repressed Conformation. PLoS One 2013;8(9).
60. Rocha-Sousa A, Hayashi T, Gomes NL, et al. A novel mutation (Cys83Tyr) in the second zinc finger of NR2E3 in enhanced S-cone syndrome. Graefes Arch Clin Exp Ophthalmol. 2011;249(2):201-8.
61. Ripamonti C, Aboshiha J, Henning GB, et al. Vision in Observers With Enhanced S-Cone Syndrome: An Excess of S-Cones but Connected Mainly to Conventional S-Cone Pathways. Invest Ophthalmol Vis Sci 2014;55(2):963-76.
62. Chen JC, Rattner A, Nathans J. The rod photoreceptor-specific nuclear receptor Nr2e3 represses transcription of multiple cone-specific genes. J Neurosci 2005;25(1):118-29.
63. Roduit R, Escher P, Schorderet DF. Mutations in the DNA-Binding Domain of NR2E3 Affect In Vivo Dimerization and Interaction with CRX. PLoS One 2009;4(10).
64. Marmor MF, Jacobson SG, Foerster MH, et al. Diagnostic Clinical Findings of a New Syndrome with Night Blindness, Maculopathy, and Enhanced S-Cone Sensitivity. Am J Ophthalmol1990;110(2):124-34.
65. Escher P, Gouras P, Roduit R, et al. Mutations in NR2E3 Can Cause Dominant or Recessive Retinal Degenerations in the Same Family. Hum Mutat 2009;30(3):342-51.
66. Bertoli F, Pignatto S, Rizzetto F, Lanzetta P. A 5-Year-Old Case of Choroidal Neovascularization in Enhanced S-Cone Syndrome Treated with Ranibizumab. Case Rep Ophthalmol 2018;9(3):510-5.
67. Broadhead GK, Grigg JR, McCluskey P, et al. Bevacizumab for choroidal neovascularisation in enhanced S-cone syndrome. Docum Ophthalmol 2016;133(2):139-43.
68. Sambricio J, Tejada-Palacios P, Barcelo-Mendiguchia A. Choroidal neovascularization, outer retinal tubulation and fundus autofluorescence findings in a patient with enhanced S-cone syndrome. Clin Exp Ophthalmol 2016;44(1):69-71.

69. Haider NB, Naggert JK, Nishina PM. Excess cone cell proliferation due to lack of a functional NR2E3 causes retinal dysplasia and degeneration in rd7/rd7 mice. Hum Mol Genet 2001;10(16):1619-26.
70. Mockel A, Perdomo Y, Stutzmann F, Letsch J, Marion V, Dollfus H. J Retinal dystrophy in Bardet-Biedl syndrome and related syndromic ciliopathies. Prog Retin Eye Res. 2011 Jul;30(4):258-74.
71. Talib M, van Schooneveld MJ, van Genderen MM, et al. Genotypic and Phenotypic Characteristics of CRB1-Associated Retinal Dystrophies A Long-Term Follow-up Study. Ophthalmology 2017;124(6):884-95.
72. den Hollander AI, ten Brink JB, de Kok YJ, et al. Mutations in a human homologue of Drosophila crumbs cause retinitis pigmentosa (RP12). Nat Genet 1999;23(2):217-21.
73. Marmor MF. Is Thioridazine Retinopathy Progressive - Relationship of Pigmentary Changes to Visual Function. Br J Ophthalmol 1990;74(12):739-42.
74. Mollema N, Haider NB. Focus on Molecules: Nuclear hormone receptor Nr2e3: Impact on retinal development and disease. Exp Eye Res 2010;91(2):116-7.
75. Ben-Yosef T, Newman H, Braverman I, et al. A combination of oculopharyngeal muscular dystrophy and a variant of enhanced S-cone syndrome in Bukharan Jews due to linked mutations in PABPN1 and NRL. Invest Ophthalmol Vis Sci 2016;57(12).
76. Littink KW, Stappers PTY, Riemslag FCC, et al. Autosomal Recessive NRL Mutations in Patients with Enhanced S-Cone Syndrome. Genes 2018;9(2).
77. Newman H, Blumen SC, Braverman I, et al. Homozygosity for a Recessive Loss-of-Function Mutation of the NRL Gene Is Associated With a Variant of Enhanced S-Cone Syndrome. Invest Ophthalmol Vis Sci 2016;57(13):5361-71.
78. Wright AF, Reddick AC, Schwartz SB, et al. Mutation analysis of NR2E3 and NRL genes in Enhanced S Cone Syndrome. Hum Mutat 2004;24(5):439.
79. Mears AJ, Kondo M, Swain PK, et al. Nrl is required for rod photoreceptor development. Nat Genet 2001;29(4):447-52.
80. Oh ECT, Cheng H, Hao H, et al. Rod differentiation factor NRL activates the expression of nuclear receptor NR2E3 to suppress the development of cone photoreceptors. Brain Res 2008;1236:16-29.
81. Farjo Q, Jackson A, PiekeDahl S, et al. Human bZIP transcription factor gene NRL: Structure, genomic sequence, and fine linkage mapping at 14q11.2 and negative mutation analysis in patients with retinal degeneration. Genomics 1997;45(2):395-401.
82. Swaroop A, Xu JZ, Pawar H, et al. A Conserved Retina-Specific Gene Encodes a Basic Motif Leucine Zipper Domain. Proc Natl Acad Sci U S A 1992;89(1):266-70.
83. Mollema NJ, Yuan Y, Jelcick AS, et al. Nuclear Receptor Rev-erb Alpha (Nr1d1) Functions in Concert with Nr2e3 to Regulate Transcriptional Networks in the Retina. PLoS One 2011;6(3)

FIGURE 1

(A) Plot of best-corrected visual acuity (BCVA, LogMar) of the right eye at baseline and last follow-up visit against patient's age. (B) Plot of BCVA (LogMar) in the right eye as a function of period of follow-up time per individual patient. (C) Plot of BCVA change in the right eye ($BCVA_{FU}$ – $BCVA_{baseline}$) as function of follow-up time (y = years) and (D) age at baseline.

FIGURE 2

Phenotypical variation of Enhanced S-Cone Syndrome in individual patients (numbered). (A) Nummular pigmentary deposition in the mid-peripheral retina. (B) Circumscribed area of nummular pigmentary deposition with halo of atrophy in inferior peripheral retina. (C) Nummular pigmentary deposition, yellow/white dots and clumped pigmentary changes in the mid-peripheral retina. (D) Yellow/white dots along vascular arcades, with increased fundus autofluorescence inside the vascular arcades, sparing the central macula. (E) Magnified view of nummular pigmentary deposition, yellow-white dots and clumped pigmentary changes in mid-peripheral retina. (F) Torpedo-like lesion in peripheral retina. (G) Subretinal fibrosis and spectral-domain optical coherence (SD-OCT) tomography across lesion (marked) showing a large subretinal hyper-reflective deposit. (H) Magnified view of yellow-white dots with early pigmentary hyperplastic changes. (I) Retinal angioma in patient with bilateral pre-retinal non-diabetic neovascularization. (J) Maculopathy, characterized by patchy atrophic macular changes, more visible on FAF. (K) Color fundus photograph of the right peripheral retina of patient 11 at baseline (right image) and 17 years later, at last follow-up (left image, year of OCT acquisition marked in left bottom corner). At baseline, retinal sclerosed vessels and yellow-white dots are seen which progressed to nummular and clumped pigmentary deposition as observed in the follow-up photograph of the same area. (L) Color fundus photograph of right superior vascular arcade in patient 15 at baseline (right image) and 11 years later, at last follow-up (left image, year of OCT acquisition marked in left bottom corner). A well-defined area of yellow-white dots is observed at baseline which developed into clumped pigmentary deposition, shown in the follow-up image.

FIGURE 3

Variation of optical coherence tomography features of Enhanced S-Cone Syndrome in individual patients (numbered). (A) Preserved foveal architecture and outer retinal atrophy, with loss of the ellipsoid zone. (B) Foveomacular schisis. (C) Magnified view of area outlined in (B), with pseudo-color representation of the the schitic cavities (round shape, in red) at the level of the inner nuclear

layer (round shape, in red) and at the level of the outer nuclear layer (elongated shape, in blue). (D) End-stage giant foveomacular schisis. (E) Disorganization of retinal layers in atrophic area of mid-peripheral retina. (F) Macular atrophy.

FIGURE 4

Macular and peripheral fundus autofluorescence (FAF) patterns in Enhanced S-Cone Syndrome in individual patients (numbered). (A) Minimal change macular FAF pattern. (B) (A) Minimal change macular FAF pattern with hyperautofluorescent flecks. (C) Mild diffuse macular hypoautofluorescence. (D) Moderate speckled macular hypoautofluorescence with increased para-macular FAF. (E) Severe end-stage macular hypoautofluorescence. (F) Peripheral hyperautofluorescent flecks. (G) Moderate diffuse (mid-peripheral half-ring or ring < 5000 µm widest diameter) peripheral hypoautofluorescence with half-ring of pronounced hyperautofluorescent ring along the temporal macular rim. (H) Near-peripheral moderate diffuse hypoautofluorescence with patchy advanced hypoautofluorescence. (I) Moderate diffuse peripheral hypoautofluorescence (> 5000 µm). (J) Advanced peripheral hypoautofluorescence. (K) Colour fundus photograph and related autofluorescence image showing the correspondence between yellow-white dots and hyperautofluorescent flecks. (L) Wide-field autofluorescence image in control subject. The macula was defined as the region encompassing 5.5 mm from the temporal margin of the optic nerve head and the mid-periphery as 3 mm around the macula.

FIGURE 5

Full-field ERG and pattern ERG (PERG) recordings from the right (RE) and left (LE) eye of a patient with Enhanced S-Cone Syndrome are compared with recordings from a representative unaffected control subject (N). ERGs include the dark-adapted (DA) ERGs (flash strengths 0.01 and 10.0 cd.s/m^2; DA 0.01 and DA 10.0) and light-adapted (LA) ERGs for a flash strength of 3.0 cd.s/m^2 (LA 3.0; 30Hz and 2Hz). The PERG is recorded to an alternating chequerboard. There is a 20ms pre-stimulus delay in single flash ERG recordings, with the exception of the S-cone ERG. Broken lines replace blink artefacts occurring after ERG b-waves, for clarity. Patient responses are superimposed to demonstrate reproducibility. In this patient the PERG P50 component is delayed but of normal amplitude. The DA0.01 ERG is undetectable. The single flash DA 3.0, DA 10.0, LA3.0 ERGs have similarly simplified and severely delayed waveforms, qualitatively comparable in shape to the S-cone ERG and consistent with generation by the same (S-cone) mechanism. The S-cone ERG is delayed and grossly enlarged. The LA30 Hz ERG is smaller than the LA 3 ERG a-wave whereas in the typical normal

subject, the LA30Hz ERG amplitude is between that of the LA3 a- and b-waves. Measurements of the main ERG components are compared with the control range in supplementary table O.

FIGURE 6

The main dark-adapted (DA) full-field ERG component amplitudes and peak times in each eye in the Enhanced S-Cone Syndrome (ESCS) cohort (filled circles and squares) and in healthy controls (grey circles) are plotted against age (in years) at the time of testing, illustrating the severity and range of ERG abnormality in the ESCS group. Data are shown for the DA strong flash (DA10) ERG a-wave amplitude (A) and peak time (B) and for the b-wave amplitude (C) and peak time (D). Regression analysis shows a similar, statistically significant ($P<0.05$) age-related reduction in amplitudes for both control (broken lines) and ESCS (solid lines) groups.

FIGURE 7

The main light-adapted (LA) full-field ERG component amplitudes and peak times in each eye in the Enhanced S-Cone Syndrome (ESCS) cohort (filled circles and squares) and in healthy controls (grey circles) are plotted against age (in years) at the time of testing, illustrating the severity and range of ERG abnormality in the ESCS group. Data are shown for the LA30 Hz flicker ERG amplitude (A) and peak time (B) and for the single flash cone (LA3) ERG a-wave amplitude (C) and peak time (D) and for the LA3 ERG b-wave amplitude (E) and peak time (F). Regression analysis shows a similar, statistically significant ($P < 0.05$) age-related reduction in amplitudes for both control (broken lines) and ESCS (solid lines) groups.

FIGURE 8

Comparison of amplitude and peak time ratios between the LA3.0 ERG a-wave and LA30Hz ERG in the Enhanced S-Cone Syndrome (ESCS) cohort (filled circles and squares) and healthy controls (open grey circles and squares). The horizontal bars show the mean +/- 1 standard deviation (SD) for amplitudes in the ESCS group. The LA30Hz ERG has an amplitude greater than the LA3 ERG a-wave in all control subjects. In ESCS the LA30Hz ERG amplitude is equal or smaller than the LA3 ERG a-wave, resulting in a ratio greater or equal to 1. *** $P = 0.0001$

FIGURE 9

The S-cone ERG component amplitudes (A) and peak times (B) are shown for the Enhanced S-Cone Syndrome (ESCS) cohort (n = 28, filled circles) and a healthy control group (n = 51, open grey circles) for comparison, plotted against age (in years). S-cone ERG amplitudes were measured from the early negative trough to maximum peak, or in the absence of an early trough from baseline to the peak of the positive polarity S-cone ERG component. The largest S-cone ERGs were seen in some of the younger ESCS individuals (solid regression line shows a negative slope) but there was no age-related statistically significant differences. Comparison of S-cone ERG amplitudes (C) and peak times (D) with those for LA3 ERG b-waves are shown for ESCS and control groups, and illustrate high positive correlation in the ESCS group, consistent with S-cone and LA3 ERGs being dominated by abnormal S-cone-opsin-mediated activity. All data relate to right eye recordings.

FIGURE 10

(A). Stereo representation of the NR2E3 ligand-binding domain (LBD) monomer (pdb code 4LOG), starting at residue 217, and locations of the novel missense NR2E3 LBD mutations mapped on the receptor. (B-D) Predicted effect of the mutations (p.R247W, p.L303P, p.R309Q) leading to a rearrangement of the bulky side chains and loss of hydrogen bonds.

Pt	Family ID	Age Onset (y)	BL	FU	Length of FU (y)	LogMar BL	FU	Variants identified
1	NA	0	49	63	14	1/1	1/1	c.119-2A>C (Hom)
2	19824	4	11	16	5	0.1/0.6	0.1/0.6	c.119-2A>C / c.1194delT; p.P399Qfs*3
3	19824	0	9	14	5	0.5/0.5	0.4/0.3	c.119-2A>C / c.1194delT; p.P399Qfs*3
4	19940	3	15	17	2	0.17/0.6	0.86/1.2	c.305C>A; p.A102D / c.767C>A; p.A256E
5	20195	3	8	14	6	0.7/0.7	1.6/1.6	c.119-2A>C / c.1194delT; p.P399Qfs*3
6	20766	4	44	49	5	0.12/0	0.17/0.17	**c.211T>C; p.F71L** / c.932G>A; p.R311Q
7	22497	5	8	11	3	0.26/0.36	0.6/0.5	NA
8	16200	6	34	48	14	0.77/0.6	1.77/1	c.119-2A>C (Hom)
9	23115	2	7	8	2	0.3/0.5	0.3/0.17	c.119-2A>C / c.1025T>C; p.V342A
10	27357	6	2.5	20	14	0.17/0.17	0.17/0.18	c.311G>A; p.R104Q (Hom)
11	15494	10	17	50	33	1.77/1.77	1.3/1.3	c.311G>A; p.R104Q (Hom)
12	27357	5	5	18	13	0.19/0.19	0/0	c.311G>A; p.R104Q (Hom)
13	3006	0	32	46	14	0.3/0.17	0.47/0.47	c.119-2A>C / c.767C>A; p.A256E
14	4644	1	13	34	21	0/0.47	0.5/0.47	c.119-2A>C (Hom)
15	16337	20	25	43	18	0.47/0.77	0.47/0.77	c.119-2A>C / c.932G>A; p.R311Q
16	15128	0	0.5	34.5	34	0.77/0.77	1.47/1	c.119-3C>G (Hom)
17	NA	6	21	35	14	0.17/2	0.17/2	NA
18	18491	20	27	35	8	0.17/0.17	0.17/0.18	c.932G>A; p.R311Q / c.1112T>G; p.L371W
19	NA	12	34	37	3	0.3/0.17	0.3/0	NA
20	20091	0	40	42	2	0.6/0.6	1/1	NA
21	18411	27	43	44	1	1/0.77	1/0.7	NA
22	NA	5	12	No FU	No FU	0.9/0.77	No FU	NA
23	20907	0	5	7.5	2.5	0.3/0.3	0.3/0.19	NA
24	19784	0	5	1	6	0.14/0	0/0	NA
25	18115	4	44	47	3	0.19/0.19	0.19/0.19	c.646G>A; p.G216S (Hom)
26	18758	4	72	81	9	0.19/0.2	0.3/0.3	c.305C>A; p.A102D (Hom)
27	NA	4	12	15	3	0.12/0	0/0	NA
28	22924	4	11	12	1	0/0	0/0	c.932G>A; p.R311Q / c.747+1G>C
29	27135	5	35	36	1	0/0.17	0.17/0.3	NA
30	22633	4	15	17	2	0.12/0	0.12/0.22	c.932G>A; p.R311Q (Hom)
31	19530	4	14	16	2	0/0	0.04/0.06	NA
32	23064	5	5	7	2	0.3/0.2	0.12/0.12	c.310C>T; p.R104W (Hom)
33	19530	4	8	10	2	0.04/0.02	0.18/0.2	NA
34	24703	12	19	21	2	0.47/1.17	0.30/0.80	c.310C>T; p.R104W (Hom)
35	19668	5	5	12	7	0.6/0.4	0.3/0.2	c.311G>A; p.R104Q / c.767C>A; p.A256E
36	18880	0	46	54	8	1/1	1/1	c.119-2A>C / **c.908T>C; p.L303P**
37	NA	20	40	45	5	0.5/0.8	0.6/1	NA
38	17494	4	20	24	4	0/0	0.1/0.2	NA
39	NA	3	11	21	10	0.3/0.3	0.4/0.4	c.119-2A>C (Hom)
40	NA	11	44	No FU	No FU	0.3/0.1	No FU	c.932G>A; p.R311Q (Hom)
41	NA	4	33	44	11	0.8/1.1	0.22/1.7	c.119-2A>C (Hom)
42	NA	5	21	27	6	0.1/0.22	0.1/0.5	c.119-2A>C / c.932G>A; p.R311Q
43	NA	4	4	10	6	0.3/0.3	0.22/0.3	c.200_208del9del; p.C67_G69del (Hom)
44	NA	3	31	No FU	No FU	0.4/0.5	No FU	c.932G>A; p.R311Q / **c.739C>T; p.R247W**
45	NA	3	11	12	4	0.22/0.1	0.22/0.1	c.932G>A; p.R311Q (Hom)
46	NA	5	46	No FU	No FU	1/0.5	No FU	c.932G>A; p.R311Q (Hom)
47	NA	5	75	76	1	0.3/2	0.4/2	c.119-2A>C / c.227G>A; p.R76Q
48	25595	12	35	36	1	0.47/0.17	0.47/0.17	c.932G>A; p.R311Q (Hom)
49	25690	3	33	No FU	No FU	0.3/0.8	No FU	c.248G>A; p.C83Y (Hom)
50	23064	8	6	2	8	0.3/0.2	0.06/0.06	c.310C>T; p.R104W (Hom)
51	25574	10	49	50	1	0.3/0.3	0.5/0.2	c.119-2A>C (Hom)
52	247	10	38	54	4.5	0.6/0.2	1/0.5	c.119-2A>C / c.932G>A; p.R311Q
53	NA	16	16	No FU	No FU	0/0	No FU	**c.926G>A; p.R309Q** (Hom)
54	NA	25	29	No FU	No FU	0/0	No FU	**c.926G>A; p.R309Q** (Hom)
55	26532	0	32	33	1	0.6/0.5	0.6/0.6	c.119-2A>C (Hom)
56	22052	0	51	55	4	1/1	1/1	c.119-2A>C (Hom)

Table 1. Clinical Data and Molecular Genetic Status of 56 Patients with Enhanced S-Cone Syndrome. Abbreviations: BL = baseline; FU = follow-up; LogMAR = logarithm of minimal angle of resolution; Hom = homozygous variant; NA = not available; Pt = patient; VA = visual acuity. Putative novel changes are shown in bold.

			LogMar			Macular changes				
Pt	**Onset (y)**	**Length of FU (y)**	**BL**	**FU**	**Progression**	**Foveomacular schisis**	**Macular oedema**	**CAI treatment**	**Macular atrophy**	**Other ophthalmic pathology**
1	0	14	1/1	1/1	N	N	N	N	Y	Senile cataracts
4	3	2	0.17/0.6	0.86/1.2	Y	Y	N	N	N	**Squint, amblyopia**
5	3	6	0.7/0.7	1.6/1.6	Y	N	Y	Y (no response)	N	
8	6	14	0.77/0.6	1.77/1	Y	Y	Y	Y (response)	Y	
11	10	33	1.77/1.77	1.3/1.3	N	Y	Y	Y (no response)	Y	
15	20	18	0.47/0.77	0.47/0.77	N	Y	Y	Y (response)	N	
16	0	34	0.77/0.77	1.47/1	Y	Y	N	N	Y (in one eye)	Congenital nystagmus
17	6	14	0.17/2	0.17/2	N	N	N	N	Y (in one eye)	**Amblyopia, retinal detachment (age 6)**
20	0	2	0.6/0.6	1/1	Y	N	N	N	N	Senile cataracts
21	27	1	1/0.77	1/0.7	N	Y	N	N	Y	
22	5	No FU	0.9/0.77	No FU	NA	Y	N	N	N	TED
34	12	2	0.47/1.17	0.30/0.80	N	Y	N	N	Y	
36	0	8	1/1	1/1	N	Y	N	N	Y	ERM, Optic nerve pallor
37	20	5	0.5/0.8	0.6/1	Y	Y	N	N	Y	
41	4	11	0.8/1.1	0.22/1.7	N	Y	Y	N	N	
46	5	No FU	1/0.5	No FU	NA	Y	N	N	N	
49	3	No FU	0.3/0.8	No FU	NA	N	N	N	Y	
56	0	4	1/1	1/1	N	Y	N	N	Y	

Table 2. Clinical characteristics of patients with severe visual impairment (LogMAR BCVA > 0.6). Significant ophthalmic events that have contributed to poor visual acuity in one eye are highlighted in bold. Abbreviations: CAI = Carbonic anydrase inhibitors; ERM = Epiretinal membrane; FU = Follow.up; N = No; NA = Not applicable; Pt = Patient; TED = Thyroid Eye Disease; Y = Yes

Pt (n)	56	
Age at presentation (median. range)	4	0-27
Age at first visit (median. range)	20.5	1-75
Age at last FU (median. range)	33	2-81
Years of FU (mean. range)	6.1	0-34
BCVA (better-seeing eye) at presentation (mean. SEM)	0.32	0.0-1.77
BCVA (better-seeing eye) at last visit (mean. SEM)	0.39	0.0-1.6
BCVA reduction (mean. SEM)	0.07	0.04
Gender		
Female gender (n. percent)	33	58.9%
Male gender (n. percent)	23	41.1%
Ethnicity		
White (n. percent)	30	53.6%
Non-White (n. percent)	26	46.4%
Refraction (n. percent)		
Plano	4	7.1%
Myopia	5	8.9%
Hyperopia	12	21.4%
NA	35	62.5%
First symptom/sign (n. percent)		
Nyctalopia	52	92.9%
Squint	9	16.1%
Nystagmus	3	5.4%
Clinical signs (n. percent)		
Optic nerve pallor	3	5.4%
Macular edema (based on structural OCT appearance)	16	28.5%
Foveomacular schisis	23	41.1%
Nummular pigmentation	48	85.7%
Yellow dots	32	57.1%
Circumferential subretinal fibrosis	4	7.1%
Torpedo-like lesions	6	10.7%
Vitreous opacities	12	21.4%
Preretinal neovascularization	1	1.8%

Table 3. Clinical characteristics of the Enhanced S-Cone Syndrome Cohort. Abbreviations: FU = follow-up; NA = not specified; Pt = patient; SEM = standard error of mean

Exon	Nucleotide Substitution and Amino Acid Change	Previous Report	InterVar Prediction	PROVEAN Prediction	Index	PolyPhen 2 Prediction	Hum Var Score (0-1)	Allelic Frequency
IVS1	c.119-2A>C	[22]			NA		NA	0.0005031
IVS1	c.119-3C>G	[33]			NA		NA	Not reported on gnomAD
2	c.211T>C; p.F71L	Novel	Uncertain significance	Deleterious	-5.218	PRD	1.00	Not reported on gnomAD
2	c.200_208del9del; p.C67_G69del	[22]		Deleterious	-26.485		NA	0.00001347
2	c.227G>A; p.R76Q	[22]	Uncertain significance	Deleterious	-3.343	PRD	1.00	0.0002140
3	c.248G>A; p.C83Y	[83]	Uncertain significance	Deleterious	-9.185	PRD	1.00	0.00001308
3	c.305C>A; p.A102D	[44]	Likely pathogenic	Deleterious	-4.862	PRD	0.99	0.00002792
3	c.310C>T; p.R104W	[22]	Uncertain significance	Deleterious	-6.962	PRD	1.00	0.00001964
5	c.646G>A; p.G216S	[22]	Uncertain significance	Neutral	0.491	Benign	0	0.00003611
5	c.311G>A; p.R104Q	[27]	Likely pathogenic	Deleterious	-3.533	PRD	1.00	0.00001964
5	c.739C>T; p.R247W	Novel	Uncertain significance	Deleterious	-7.733	PRD	1.00	Not reported on gnomAD
6	c.908T>C; p.L303P	Novel	Uncertain significance	Deleterious	-6.552	PRD	1.00	Not reported on gnomAD
6	c.932G>A; p.R311Q	[22]	Likely pathogenic	Neutral	-1.831	PSD	0.627	0.0004071
6	c.767C>A; p.A256E	[84]	Likely pathogenic	Deleterious	-3.659	PRD	0.998	0.00003715
6	c.926G>A; p.R309Q	Novel	Likely pathogenic	Deleterious	-3.520	PRD	0.959	0.00001528
7	c.1025T>C; p.V342A	[85]	Uncertain significance	Deleterious	-3.677	PRD	0.996	Not reported on gnomAD
8	c.1194delT; p.P399Qfs*3	[85]			NA		NA	Not reported on gnomAD
8	c.1112T>G; p.L371W	[86]	Uncertain significance	Deleterious	-5.107	PRD	1.00	Not reported on gnomAD

Table 4. NR2E3 variants. gnomAD = Genome Aggregation Database; Hum Var Score = human variation score; InterVar = Clinical Interpretation of Genetic Variants by the 2015 ACMG-AMP Guidelines, which categorizes causality of variants as pathogenic, likely pathogenic, uncertain significance, likely benign, and benign [http:// http://wintervar.wglab.org. Accessed June 12, 2020]. NA = not applicable; PRD = probably damaging; PSD = Possibly damaging; PROVEAN = Protein Variation Effect Analyzer [http://provean.jcvi.org/index.php. Accessed February 15, 2019]. Variants with a score equal to or below -2.5 are considered "deleterious". Variants with a score above -2.5 are considered "neutral". Polyphen 2 (vision 2.1) appraises mutations qualitatively as benign, possibly damaging or probably damaging based on the model's false positive rate [http://genetics.bwh.harvard.edu/pph2/. Accessed February 28, 2020]. HumanVar-trained model of Polyphen 2 was selected,

since diagnostics of mendelian diseases requires distinguishing mutations with drastic effects from all the remaining human variation, including abundant mildly deleterious alleles.

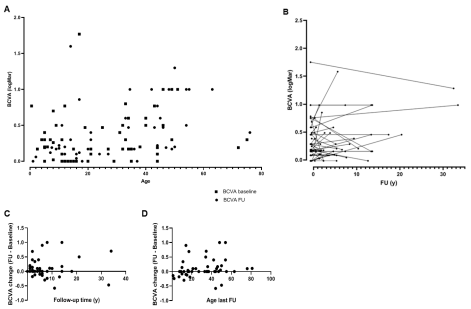

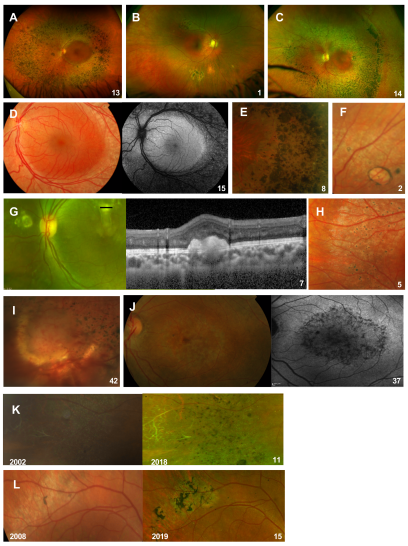

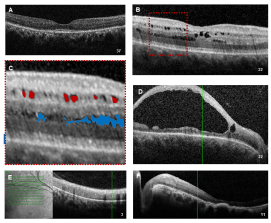

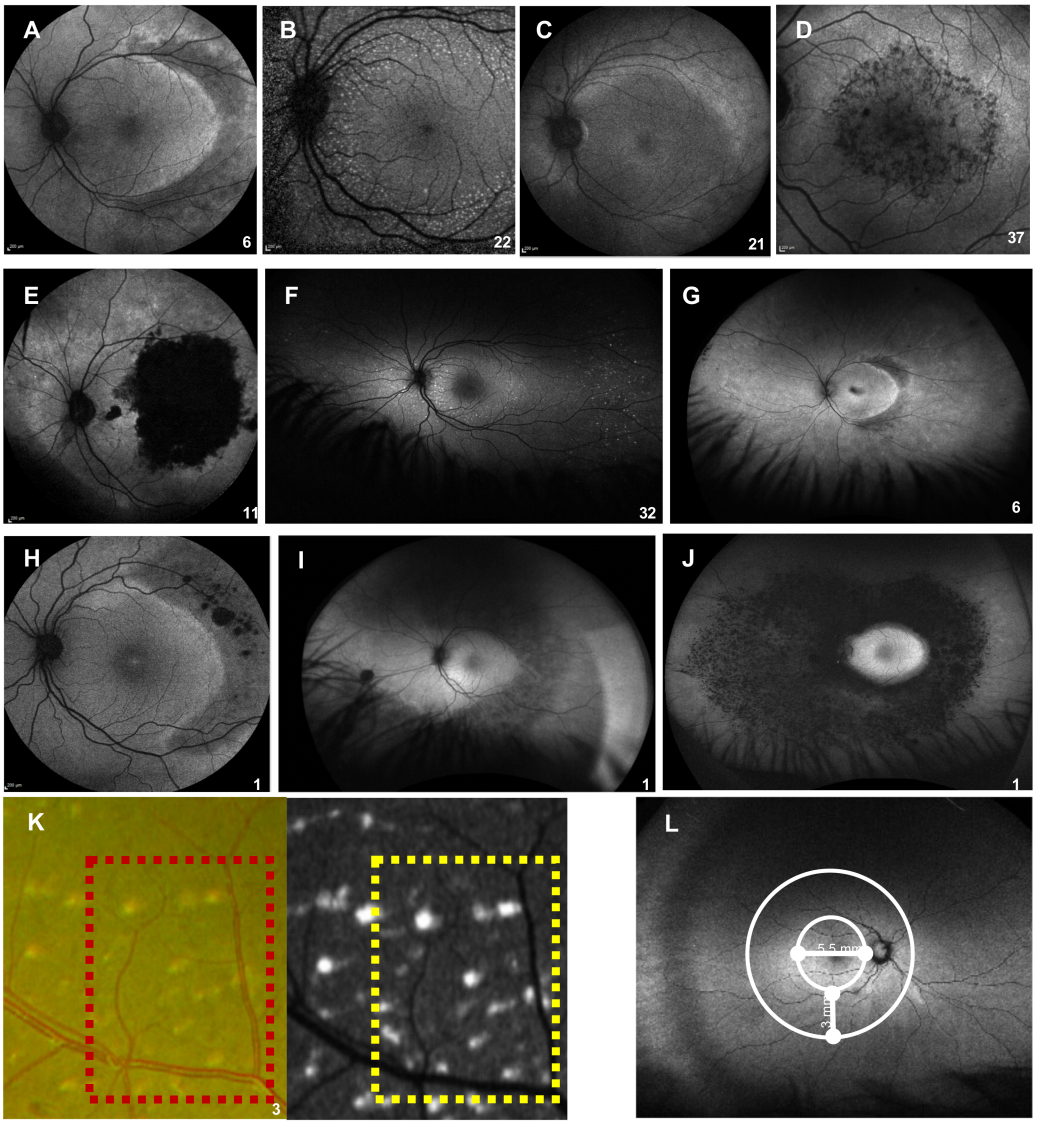
A
6
B
22
C
21
D
37
E
11
F
32
G
6
H
1
I
1
J
1
K
3
L
5.5 mm
3 mm

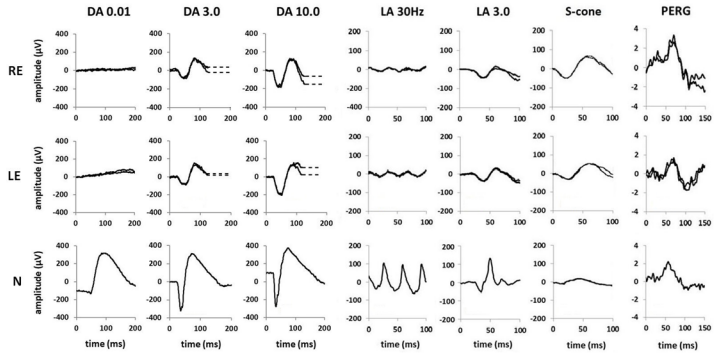

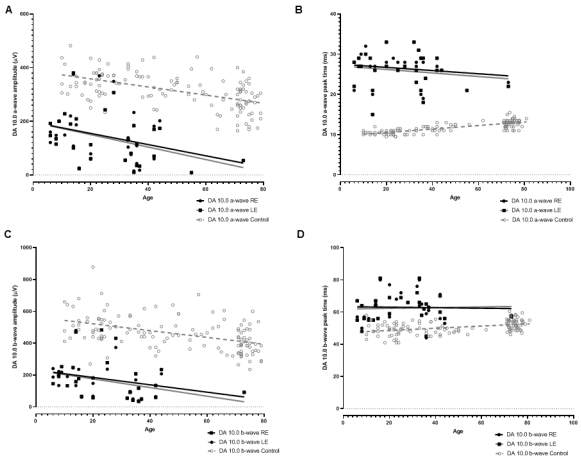

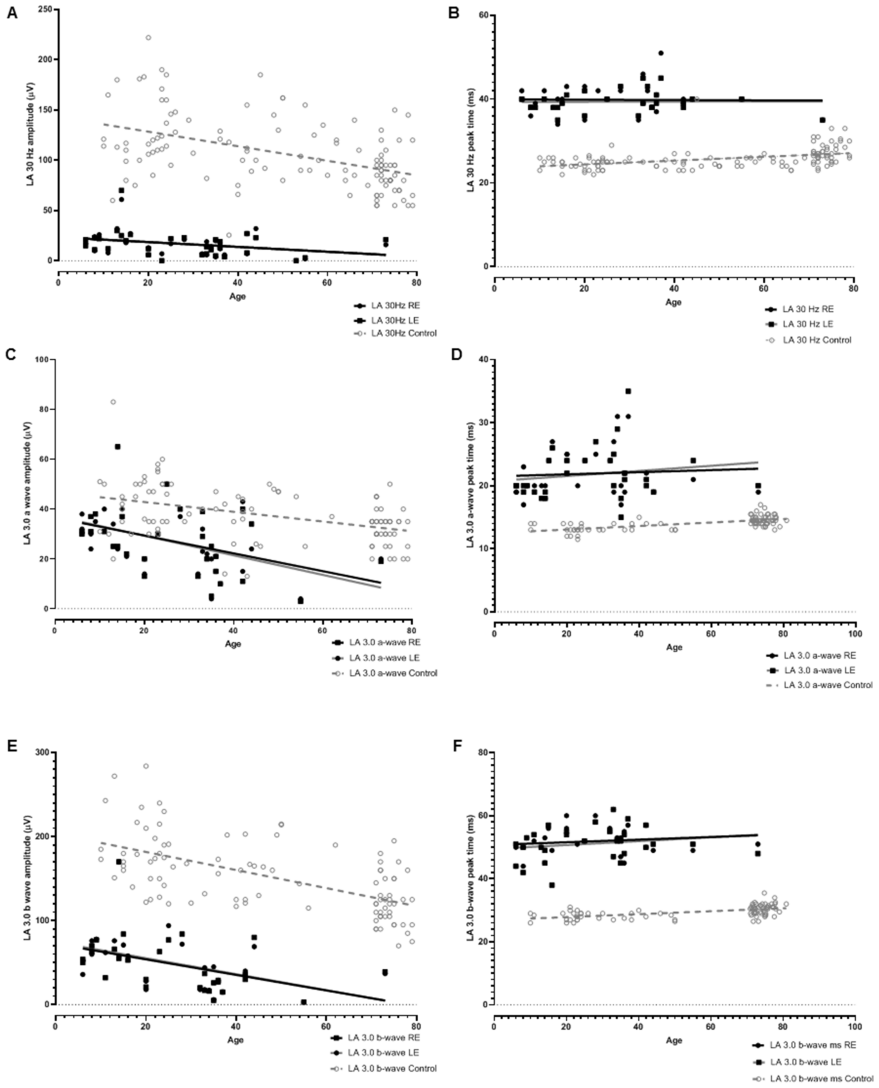
A
LA 30 Hz amplitude (µV)
Age
LA 30Hz RE
LA 30Hz LE
LA 30Hz Control
B
LA 30 Hz peak time (ms)
Age
LA 30 Hz RE
LA 30 Hz LE
LA 30 Hz Control
C
LA 3.0 a wave amplitude (µV)
Age
LA 3.0 a-wave RE
LA 3.0 a-wave LE
LA 3.0 a-wave Control
D
LA 3.0 a-wave peak time (ms)
Age
LA 3.0 a-wave RE
LA 3.0 a-wave LE
LA 3.0 a-wave Control
E
LA 3.0 b wave amplitude (µV)
Age
LA 3.0 b-wave RE
LA 3.0 b-wave LE
LA 3.0 b-wave Control
F
LA 3.0 b-wave peak time (ms)
Age
LA 3.0 b-wave ms RE
LA 3.0 b-wave LE
LA 3.0 b-wave ms Control

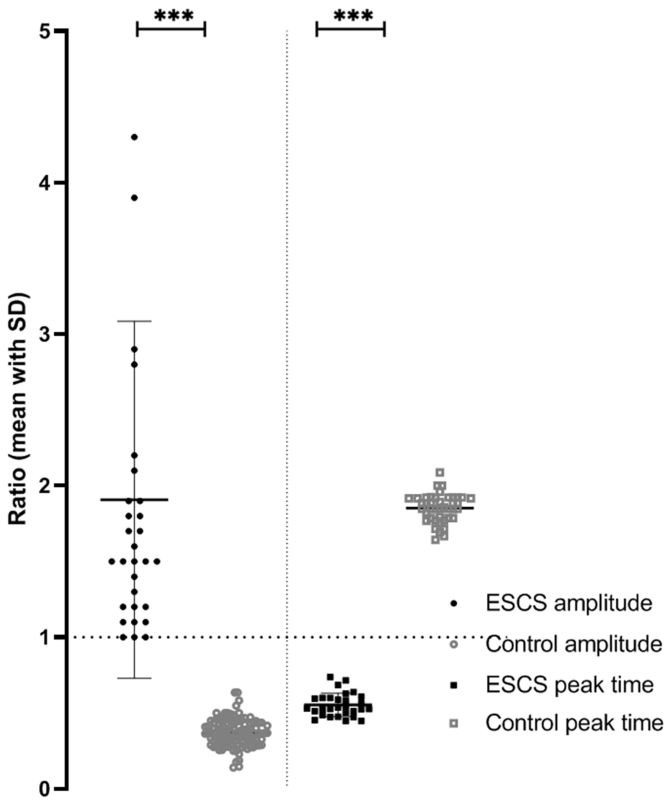

$$Ratio = \frac{Photopic\ a-wave}{30\ Hz}$$

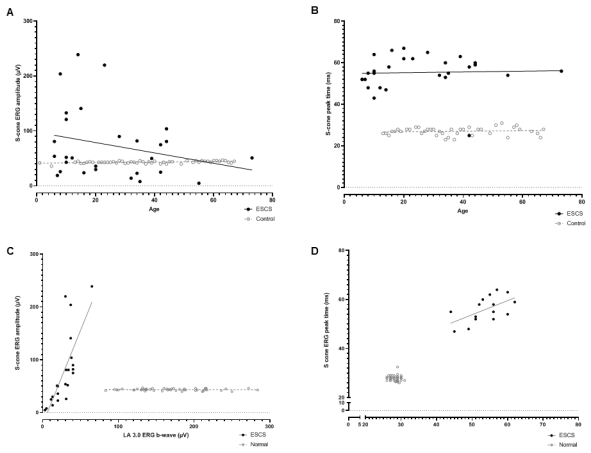

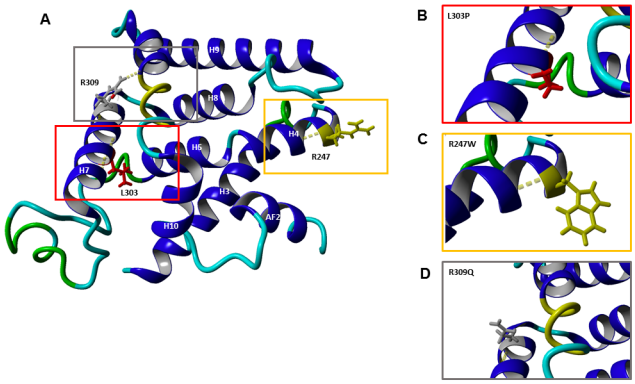

Précis

Enhanced S-Cone Syndrome, caused by mutations in the *NR2E3* gene, has a variable clinical phenotype and typical electrophysiological responses that are relatively stable over time.